Geogrid installation damage caused by recycled construction and demolition waste

M. P. Fleury[1], E. C. G. Santos[2], J. Lins da Silva[3] and E. M. Palmeira[4]

[1] *PhD student, Department of Geotechnical Engineering, São Carlos School of Engineering, University of São Paulo (USP), São Carlos, Brazil, E-mail: mateusfleury@usp.br (Orcid:0000-0002-8493-5991)*
[2] *Assistant Professor, Department of Civil and Environmental Engineering, Federal University of Goiás (UFG), Goiânia, GO, Brazil, E-mail: edersantos@ufg.br (corresponding author) (Orcid:0000-0002-4137-9921)*
[3] *Assistant Professor, São Carlos School of Engineering, University of São Paulo (USP), São Carlos, Brazil, E-mail: jefferson@sc.usp.br (Orcid:0000-0002-2226-4950)*
[4] *Professor, Department of Civil and Environmental Engineering, University of Brasilia (UnB), Brasilia, Brazil, E-mail: palmeira@unb.br (Orcid:0000-0003-2620-0708)*

Received 14 January 2019, revised 02 April 2019, accepted 18 August 2019, published 11 October 2019

ABSTRACT: Using recycled construction and demolition waste (RCDW) in geosynthetic reinforced soil (GRS) structures presents attractive environmental and economic aspects. However, bearing in mind installation damage can be responsible for significant changes in geosynthetic tensile-strain behavior, the damage caused by the RCDW must be assessed and quantified. This study aims to investigate the occurrence of mechanical damage during the installation of geogrids with RCDW backfill material using an in-field test facility. In order to understand the mechanisms related to the damage, the influences of the dropping height and compaction method were investigated. Statistical analysis using the Student's *t*-distribution was carried out to validate the occurrence of damage and calculate reduction factors for geogrids' tensile strengths. Results revealed that dropping processes reduced the geogrid ultimate tensile strengths, but the compaction methods caused the highest reductions. The reduction factor values encourage the design of GRS structures with RCDW, an interesting option to satisfy the technical and economic aspects required for these structures in agreement with the environmental concerns.

KEYWORDS: Geosynthetics, mechanical damage, recycled construction and demolition waste, dropping height, compaction methods, reduction factors

REFERENCE: Fleury, M. P., Santos, E. C. G., Lins da Silva, J. and Palmeira, E. M. (2019). Geogrid installation damage caused by recycled construction and demolition waste. *Geosynthetics International*, **26**, No. 6, 641–656. [https://doi.org/10.1680/jgein.19.00050]

1. INTRODUCTION

Reinforcement material durability is an important issue related to the design of geosynthetic reinforced soil (GRS) structures. Among the factors affecting polymeric material durability, installation damage (i.e. mechanical damage) can be classified as the most critical mechanism (Hufenus *et al*. 2005). When related to geogrids, this damage is responsible for changes in ultimate tensile strength (T_{ult}), strain at failure (ε_f) and secant tensile stiffness (J_{sec}) and can affect the behaviour of the GRS structures. Hence, installation damage investigations have been carried out over the last decades (Koerner and Koerner 1990).

Furthermore, the application of non-conventional backfill materials in GRS structures favours the concept of sustainable development required by modern engineering. Facing the significant amount of construction and demolition waste (CDW) generated, a proper management strategy, such as recycling, creates new raw materials for geotechnical applications. However, approximately 23% of Brazilian recycling plants do not carry out or have never carried out technical characterisation in their products (Brazilian Association for the Recycling of Construction and Demolition Waste; ABRECON 2015). Despite the regional variability of recycled construction and demolition waste (RCDW) technical characteristics (Ossa *et al*. 2016), mainly due to different construction processes adopted around the world, recent studies have shown that RCDW has the potential to be an alternative filling material in GRS structures (Santos *et al*. 2013, 2014; Arulrajah *et al*. 2014; Vieira and Pereira 2015a, 2015b, 2016; Cardoso *et al*. 2016; Vieira *et al*. 2016; Soleimanbeigi *et al*. 2019). Therefore, the composite (RCDW and geogrids) applied in GRS structures seems

to satisfy both environmental and technical aspects required by the concept of sustainable development (Basu *et al*. 2014; Correia *et al*. 2016; Damians *et al*. 2017, 2018).

However, installation damage caused by RCDW to geogrids must be evaluated and quantified in order to provide suitable design parameters. In the literature, the investigation of mechanical damage caused by the compaction procedures for different types of backfilling materials (natural and recycled) has already been investigated (Richardson 1998; Hufenus *et al*. 2005; Santos *et al*. 2012; Lim and McCartney 2013; Pinho-Lopes and Lopes 2014; Vieira and Pereira 2015a). Nevertheless, there is limited information about the influence of the dropping process in geogrids' reduction tensile strength. This paper fills this gap, aiming to evaluate and quantify the installation damage caused by RCDW to geogrids. Through a statistical evaluation and simulations of dropping and compaction mechanisms, individual and synergy effects to geogrids' short-term mechanical behaviour were assessed in terms of ultimate tensile strength, secant tensile stiffness and strain at failure. Finally, the paper provides the characterisation of RCDW produced in Brazil to make their geotechnical characteristics widespread.

2. BACKGROUND

Over the last decades, the application of geogrids has increased worldwide due to their advantages related to mechanical characteristics, construction process and competitive costs. In this context, the extended lifetime of GRS structures and the uncertainty about the mechanical properties of reinforcement elements over their lifetime point out the durability of geogrids as an essential issue to designers (Richardson 1998; Huang and Chiou 2006). Mechanical damage leads to an immediate reduction in the geogrids' tensile strength (Rosete *et al*. 2013). Damage is also suffered during geogrid installation (in the handling, transportation, dropping, strewing and compaction processes of the backfill materials) and under its service conditions or repeated loads (Hufenus *et al*. 2005; Huang 2006). However, installation damage represents the most critical harm caused to a geosynthetic reinforcement during its lifetime (Hufenus *et al*. 2005).

To deal with the damage caused by installation activities, GRS structure designers consider the application of an installation damage reduction factor (RF_{ID}) to determine the geosynthetic allowable tensile strength (T_{al}), according to (Allen and Bathurst 1996)

$$T_{al} = \frac{T_{ult}}{RF} = \frac{T_{ult}}{RF_{ID} \cdot RF_{CR} \cdot RF_{D}} \quad (1)$$

where T_{ult} is the ultimate tensile strength; RF, the global reduction factor; RF_{CR}, the creep reduction factor; and RF_D is the durability reduction factor. The RF_{ID} is calculated according to:

$$RF_{ID} = \bar{T}_{ult\_v} / \bar{T}_{ult\_d} \quad (2)$$

where $\bar{T}_{ult\_v}$ and $\bar{T}_{ult\_d}$ represent the ultimate tensile strength mean value of virgin (undamaged) and damaged specimens, respectively.

Equation (1) is applicable for allowable stress design and limit state design. For the latter, the use of reliability base analysis is important to calibrate load and resistance factors. Considering natural aggregates, calibrations with a large amount of data have been performed in terms of installation damage (Bathurst *et al*. 2011; Miyata and Bathurst 2015), creep rupture (Bathurst *et al*. 2012) and for the synergy between them (Bathurst and Miyata 2015). However, adopting reliability base analysis for calibrating reduction factors caused by recycled aggregates is not within the scope of this study.

Over the last decades, researchers have carried out many investigations to determine RF_{ID} values for different conditions, adopting the following sequence: installation damage simulation (in-field or laboratory tests); tensile strength tests on virgin and damaged specimens; visual inspections; determination of RF_{ID}; and correlation between RF_{ID} and visual inspections.

Some authors (Paula *et al*. 2004; Huang 2006; Huang and Chiou 2006; Huang and Wang 2007; Yoo *et al*. 2009; Rosete *et al*. 2013; Gonzalez-Torre *et al*. 2014) performed the standard laboratory test EN ISO 10722:2007 (BSI 2007) focused on evaluating the mechanical damage to geogrids under repeated loading with granular materials. The values of RF_{ID}, for different repeated loads and granular materials, varied from 0.93 to 1.54.

In general, the results revealed: values of RF_{ID} became higher as the cyclic load intensity increased (Huang and Chiou 2006; Huang and Wang 2007; Rosete *et al*. 2013; Pinho-Lopes and Lopes 2014); the synthetic aggregate (sintered aluminium dioxide) produced more damage than natural aggregates with similar grain size distributions (Paula *et al*. 2004); tests with fine grained materials (as the standard synthetic aggregate) underestimate the damage compared with tests performed with coarser materials (Huang 2006; Huang and Chiou 2006; Pinho-Lopes and Lopes 2014); and the grain size distribution of natural aggregates impacted the values of RF_{ID} (Yoo *et al*. 2009; Lim and McCartney 2013). Huang and Liao (2007) investigated damage caused by turbid flow and highlighted the coating material effects on geosynthetics' resistance to mechanical damage. Huang and Chiou (2006) associated the damage effect with the ratio of coating material volume and the mass of yarns (V-M ratio). Rosete *et al*. (2013) recommended adopting cumulative effects of abrasion and repeated load damage instead of multiplying independent RF_{ID}.

Despite the contribution made by laboratory tests, adoption of full-scale tests has been recommended when coarse particles are present in backfill materials to better represent installation procedures (Hufenus *et al*. 2005; Huang 2006; Huang and Wang 2007). In-field investigations of installation damage to geogrids using gravel and coarse backfill materials revealed values of RF_{ID} from 0.87 to 2.33 (Austin 1997; Richardson 1998; Hsieh and Wu 2001; Hufenus *et al*. 2002, 2005; Cho *et al*. 2006; Jeon and Bouazza 2010; Paula *et al*. 2012; Lim

and McCartney 2013; Pinho-Lopes and Lopes 2014; Pinho-Lopes *et al*. 2018). Studies carried out using RCDW found values of RF_{ID} from 0.94 to 1.28 (Santos *et al*. 2012; Vieira and Pereira 2015a).

The wide range of values of RF_{ID} obtained from in-field investigation and laboratory tests are a result of different test conditions. Nevertheless, these different tests identified several factors affecting installation damage. Hufenus *et al*. (2005) and Pinho-Lopes and Lopes (2014) pointed out that the geosynthetic type is a primary factor to be considered. Focusing on geogrids, high-density polymeric materials (e.g. HDPE and HDPP) are more resistant to installation damage (Austin 1997; Cho *et al*. 2006; Jeon and Bouazza 2010; Lim and McCartney 2013). More severe damage was observed when gravel and angular particles comprised the backfill material (Hsieh and Wu 2001; Cho *et al*. 2006; Jeon and Bouazza 2010; Paula *et al*. 2012; Lim and McCartney 2013). However, Pinho-Lopes and Lopes (2014) verified greater damage with fine-grained soil than in gravel. These results suggest an influence of backfill material gradation. Hufenus *et al*. (2002) and Lim and McCartney (2013) highlighted the negligible influence of compaction thickness, but Richardson (1998) suggested adopting layer thicknesses higher than 150 mm or four times the maximum backfill material particle size.

International standards recommend using granular and non-plastic materials in GRS structures (BS 8006-1 (BSI 2010); FHWA 2010; NCMA 2010; EBGEO 2011). According to Santos and Vilar (2008), these specifications make it possible to use alternative backfill materials, such as recycled construction and demolition waste (RCDW), as those geotechnical characteristics are achieved. In this scenario, adopting proper management actions and recycling procedures could enable the return of a significant amount of recycled materials to the construction industry as raw material (e.g. backfill materials in geotechnical engineering).

Besides the environmental benefits related to using RCDW, several authors also studied their technical properties for different applications: pavements (Niekerk *et al*. 2002; Poon and Chan 2006; Leite *et al*. 2011; Herrador *et al*. 2012; Taherkhani 2015; Ossa *et al*. 2016); concrete (Nagataki *et al*. 2004; Brito *et al*. 2005; Silva *et al*. 2014); and GRS (Santos *et al*. 2009, 2010, 2013, 2014; Arulrajah *et al*. 2014; Vieira and Pereira 2015a, 2016; Vieira *et al*. 2016; Soleimanbeigi *et al*. 2019). Moreover, two instrumented wrapped-face geosynthetic reinforced walls with RCDW backfill material demonstrated satisfactory performance – quite similar to that expected for GRS built with conventional materials – (Santos *et al*. 2013) and supported the deformations caused by an induced inundation of their collapsible foundation soil (Santos *et al*. 2014).

To promote the use of RCDW in GRS structures, some authors have investigated installation damage caused by these materials in geogrids. Santos *et al*. (2012) verified higher values of RF_{ID} caused by compaction processes when they were carried out using a vibratory hammer compared to those caused by a lightweight roller (without vibratory movements). Vieira and Pereira (2015a) did not find significant damage when a compaction plate was used for compaction. Barbosa and Santos (2013) and Barbosa *et al*. (2016) investigated the influence of the synergy between the dropping process and compaction procedures. The authors reported higher RF_{ID} values for the scenario involving a 1.0 m dropping height compared to the scenario with a 2.0 m dropping height.

In order to improve knowledge of geogrid installation damage and to help with better design parameters for RCDW application in GRS structures, this study focused on evaluating the damage caused by the backfill dropping process (height), different compaction procedures, and the synergy between these two processes.

3. MATERIALS AND METHODS

3.1. Recycled construction and demolition waste (RCDW)

The RCDW used in this investigation was provided by a recycling plant in Aparecida de Goiânia-GO, in the metropolitan region of Goiânia-GO (capital city of the state of Goiás). The recycling plant used a jaw crusher to reduce the particle size of CDW in a single process. Due to the construction methods normally adopted in Brazil, the CDW that arrives at the recycling plant mainly consists of concrete, masonry and mortar. The RCDW used in this study comprises similar volumes of four particle size (d) recycled products: gravel ($d > 19$ mm), gravel A (19 mm $< d <$ 9.5 mm), gravel B (9.5 mm $< d <$ 4.8 mm) and sand ($d < 4.8$ mm). However, it is important to pay attention to the fact that particle breakage can occur during the mixing procedure, which may affect the grain size distribution curve of the final RCDW product.

In order to evaluate the variability of RCDW properties, five samples – codes RCDW 01 to 05 – were collected in 15-day intervals and a sampling procedure was carried out in different parts of the waste pile (bottom, middle and top). The laboratory tests consisted of specific gravity (G_s); grain-size distribution; Atterberg limits; compaction test (Standard Proctor); and a composition test. The composition test followed similar procedures to those adopted by Santos (2007), where 10 kg of RCDW were sieved (mesh aperture 4.76 mm) under running water – the RCDW passing in mesh #4 is considered 'soil particles' – and the retained RCDW, after 12 h of oven drying, is sorted by visual analysis (naked eye).

3.2. Characteristics of geogrids

This study evaluated the performance of three geogrids usually used in GRS structures (Figure 1). The decision to adopt two geogrids with polyester filaments (PET-35, mass per unit area, $M_A = 185$ g/m^2; and PET-55, $M_A = 280$ g/m^2) and one geogrid with polyvinyl alcohol filaments (PVA-35, $M_A = 160$ g/m^2) was made in order to check the influences of the constitutive polymers and tensile strengths on installation damage. According to the manufacturer, all geogrids have less than 10% strain at ultimate tensile strength. For in-field tests, each type of

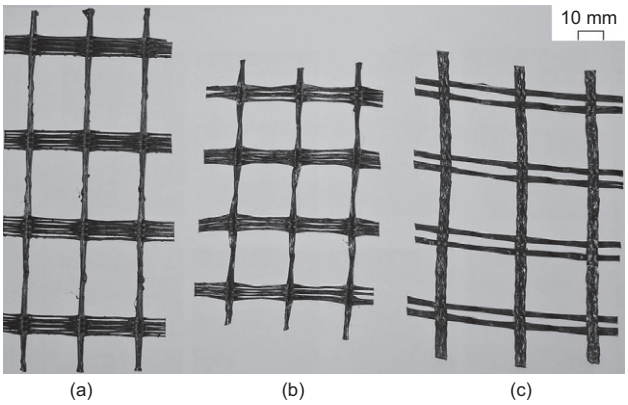

Figure 1. Geogrids: (a) PVA-35, (b) PET-35 and (c) PET-55

geogrid was cut into four meshes of 1.2 m by 3.90 m (longitudinal and transversal directions, respectively).

3.3. Installation damage program

3.3.1. *Experimental facility construction*

The construction of an experimental facility measuring 8.0 m long by 3.9 m wide was carried out to investigate the installation damage caused by RCDW to the geogrids. The facility consists of a reinforced concrete base (60 mm thick); precast concrete beams (responsible for retaining the RCDW laterally); and a pyramidal plastic tent to protect the experiment from rainfall (at least 3 m from the ground). Figure 2 shows the experimental facility cross-section drawing and its view can be seen in the supplementary material available on the journal website.

3.3.2. *Installation damage simulation*

This study assessed the influence of installation damage related to the dropping process and compaction methods used on the filling material (RCDW). The dropping process occurred at three different heights: 0.0 m (H0), 1.0 m (H1) and 2.0 m (H2). Concerning this process, another scenario was evaluated: RCDW dropping from a 2.0 m height over a 50-mm thick RCDW layer (protection layer) placed above the geogrid – this configuration was called H2*. Three compaction methods were investigated: no compaction (NC), to evaluate the influence of the dropping process; compaction with a vibratory roller (VR) with a 1400 kg operational weight distributed on a 900 mm roller length; and compaction using a vibratory hammer (VH) with a 74 kg operational weight over a 320 × 280 mm plate.

Once the dropping process (four scenarios) and compaction methods (three scenarios) were performed on three geogrid types, 36 scenarios were evaluated in total (12 per each geogrid). The nomeclatures used for the scenario show the whole condition investigated. For example, the PVA-35-H1-VH scenario implies a test on a geogrid of polyvinyl alcohol filaments and tensile strength of 35 kN/m, with RCDW dropping from a height equal to 1.0 m (H1) and compacted with the vibratory hammer (VH).

The in-field experimental facility area was divided to optimise the simulations of installation damage. Six types of meshes (1.2 m × 3.9 m) were placed and arranged with 100 mm space (Figure 3). Three scenarios were evaluated for each geogrid mesh. Each scenario occupied an area of 1.2 m by 1.3 m in the longitudinal and transversal directions, respectively. The in-field experimental facility was used twice, nominated as 'condition A' for the first filling and 'condition B' for the second filling, to perform all the scenarios investigated. Figure 3 presents the scenarios investigated in the field site conditions (A and B) for each type of geogrid.

3.3.3. *Test procedure sequence*

The first process consisted of compaction (four roller passes) of a 100 mm thick RCDW layer – called the 'bottom RCDW layer' – over the reinforced concrete base. Then, geogrid meshes were laid over the bottom RCDW layer according to section 3.3.2. To avoid damage induced by dropping in adjacent specimens, a wooden board (50 mm thick) was laid over the geogrids. For scenario H2* (2.0 m dropping height over 50 mm RCDW thickness layer), the RCDW protective layer was spread using a hoe and shovel. The process for positioning the wooden board and spreading the protective layer can be found in the supplementary material available on the journal's website. Once the dropping process ended and the in-field experimental facility was filled, the top RCDW layer was compacted to reach a 200 mm layer thickness (six vibratory roller passes or eight vibratory hammer passes). In the end, a 300 mm GRS layer was constructed with a final configuration as presented in Figure 2. Similar procedures were carried out by Austin (1997), Hufenus

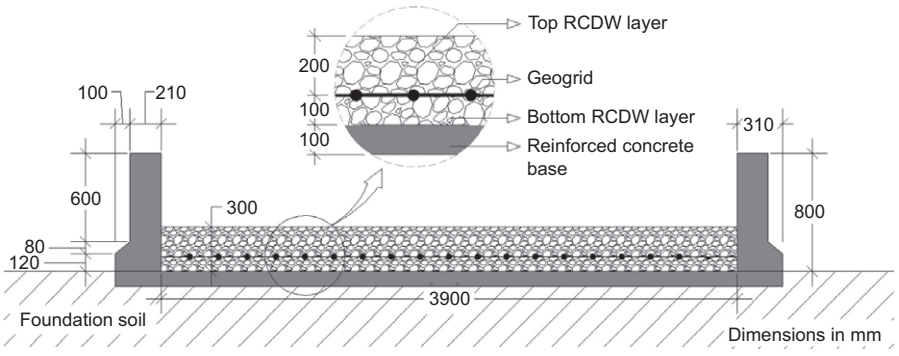

Figure 2. In-field test facility cross section

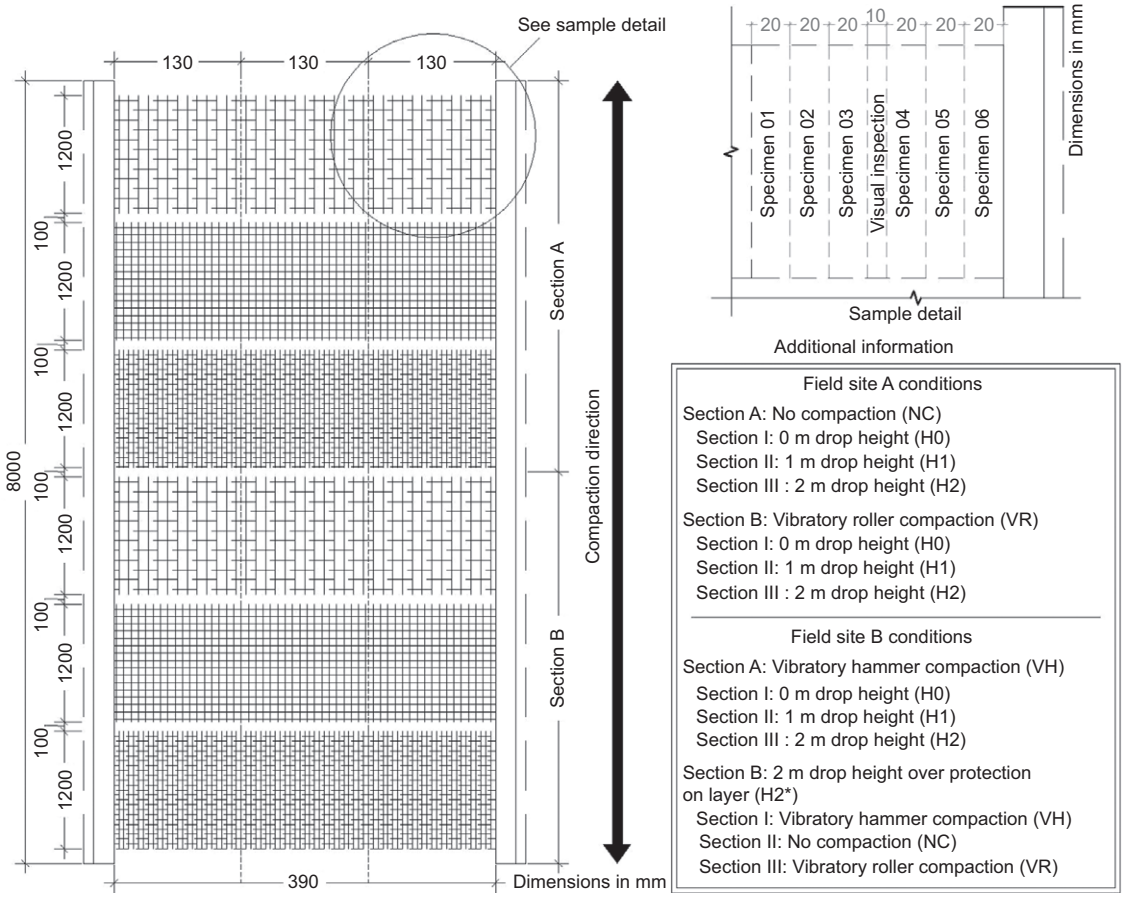

Figure 3. In-field facility plant (with sample detail and additional information table)

et al. (2002, 2005), Cho *et al*. (2006), Jeon and Bouazza (2010) and Lim and McCartney (2013) for conventional backfill materials, and by Santos *et al*. (2012), Barbosa and Santos (2013) and Vieira and Pereira (2015a) for RCDW backfill materials.

3.3.4. *Exhumation and geogrid specimen preparations*
After the damage simulations, the geogrid samples (1.2 m long and 1.3 m wide) were exhumed manually with a shovel and hoe. Two samples of RCDW were collected during the exhumation process, one related to Condition A, identified as 'RCDW 06', and another related to Condition B, identified as 'RCDW 07'.

The geogrid specimens were tested in the Geosynthetic Laboratory at the University of São Paulo (USP) in São Carlos, state of São Paulo, Brazil, for tensile strength tests according to ASTM D 6637-15 using electromechanical equipment (Instron 3385H) with a video-extensometer. Each geogrid sample was divided into seven specimens (Figure 3, see sampling detail). Six were prepared for tensile strength tests (1.2 m × 0.2 m), and one for optical microscope inspection (1.2 m × 0.1 m). Although six specimens were available for tensile strength tests, only five were tested for the investigated scenario (virgin and damaged). Specimen #06 was kept as a control specimen. The results from the optical microscope inspection are not presented in this paper and further analysis will be performed for future publications.

3.4. Validation and quantification of damage

Before installation damage was quantified, a statistical analysis was carried out to validate the damage that occurred based on determining the confidence intervals of the properties of interest (T_{ult}, ε_f, and J_{sec}) of virgin specimens. To do that, the Student's *t*-distribution was adopted, given that this distribution is used for estimating the mean of a normally distributed population in situations where the sample size is small, and the population standard deviation is unknown. According to the Student's *t*-distribution, the sample mean value confidence is given by

$$t = \frac{\bar{X} - \mu}{S/\sqrt{n}} \tag{3}$$

where t is the value of the Student's *t*-distribution variable, $\bar{X}$ is the mean value of the virgin sample; μ, the population mean; S, sample standard deviation; and n is the sample size.

Quantification of the installation damage was measured based on calculating reduction factors related to ultimate tensile strength (RF_{T_ult}), strain at failure (RF_{ε_f}), and secant tensile stiffness at 2% and 5% strain (RF_{J_sec2} and RF_{J_sec5}, respectively). To validate the occurrence of damage, the following analysis was carried out.

The damaged sample mean value ($\bar{X}_d$) into the virgin sample confidence level interval (calculated according to Student's *t*-distribution): this scenario raises doubts about

the occurrence of damage, and hence the reduction factor was assumed as equal to 1.0.

Damaged sample mean value ($\bar{X}_d$) out of the virgin sample confidence level interval: for this scenario, the reduction factor was calculated according to

$$RF_X = \frac{\bar{X}}{\bar{X}_d} \quad (4)$$

where, RF_X is the reduction factor related to the X parameter, $\bar{X}$ is the virgin sample mean value of the analysed parameter and $\bar{X}_d$ is the damaged sample mean value of the analysed parameter.

4. RESULTS AND DISCUSSION

4.1. Recycled construction and demolition waste (RCDW)

The results of composition tests (Table 1) showed the predominance of soil, concrete, mortar and ceramic, in that order. These results reveal that RCDW is mainly composed of inert materials. These components, together with weathered rock and polished ceramic contents, compose more than 98% in all RCDW samples analysed. Similar results were reported by Santos *et al*. (2010), Leite *et al*. (2011) and Vieira and Pereira (2015b, 2016).

Particles of RCDW smaller than 4.75 mm presented specific gravity results with low variability (Table 2). A mean value of 1.811 and a coefficient of variation (COV) equal to 2.49% were obtained. The controlled recycling process adopted by the recycling plant and CDW generation with similar composition in the region are pointed out as responsible for these results. However, further investigations are required for particles bigger than 4.75 mm, since the composition results (Table 1) revealed considerable variability of materials (i.e. concrete, mortar and ceramic) in the samples. Recycling procedures, the quality of the original material (CDW) and the particle sizes are factors that affect the density/specific gravity of RCDW aggregates (Silva *et al*. 2014).

The grain size distribution curves (Figure 4a) indicate a considerable variability, which makes the best representation of the RCDW grain size distribution given by a 'grain size distribution range' (hereafter called RCDW range). Sample RCDW 5 greatly influenced this variability, with a COV higher than 5.0% in the range limited by soil particles of 0.01 mm and 9 mm. The samples' composition, particularly that of the soil, concrete and mortar contents, was an influential factor related to the shape of the grain size distribution curves. Sample RCDW 05 – the predominant bottom curve in Figure 4a – showed the lowest soil content (35.18%) and the highest value of concrete and mortar content summed (hereafter called cement products; 51.54%). On the other hand, sample RCDW 07 – the upper curve in Figure 4a – presented the highest soil content (60.41%) and lowest cement product content (36.07%). In this context, the shapes of the grain size distribution curves of RCDW 03 and RCDW 04 overlap because of the similar soil and cement product

Table 1. RCDW composition in percentage by weight

Component	RCDW 01	RCDW 02	RCDW 03	RCDW 04	RCDW 05	RCDW 06	RCDW 07
Soil	47.38	57.85	51.47	52.71	35.18	58.97	60.41
Concrete	40.42	18.44	30.58	24.92	25.68	27.27	24.15
Mortar	8.39	17.24	12.97	15.69	25.86	9.24	11.92
Ceramic	1.51	2.83	2.72	3.60	5.99	2.25	1.61
Weathered rock	1.50	1.11	1.15	1.63	2.49	0.87	1.02
Polished ceramic	0.18	1.39	0.48	0.59	3.09	1.05	0.56
Others[a]	0.62	1.14	0.63	0.86	1.71	1.40	0.33

[a]Includes bituminous materials, fabric, glass, metal, plaster, plastic and wood.

Table 2. Summary of RCDW characterisation results

Characteristics	RCDW 01	RCDW 02	RCDW 03	RCDW 04	RCDW 05	RCDW 06	RCDW 07
G_s[a]	2.677	2.676	2.699	2.693	2.693	2.718	2.714
PI[b]	NP[c]	NP[c]	NP[c]	NP[c]	NP[c]	NP[c]	NP[c]
USCS[d]	GW-GM[e]	SP-SM[f]	SP-SM[f]	SP-SM[f]	GP-GM[g]	SP-SM[f]	SP-SM[f]
$\gamma_{d\_máx}$ (kN/m^3)[h]	18.96	18.08	18.37	17.66	18.09	17.65	17.99
w_{op} (%)[i]	12.4	15.1	15.0	15.4	15.8	15.4	13.0

[a]Specific gravity of grains passing through 4.76 mm sieve.
[b]Plasticity index.
[c]Non-plastic behaviour.
[d]Unified Soil Classification System according to ASTM D 2487-06.
[e]Well-graded gravel with silt
[f]Poorly-graded sand with silt
[g]Poorly-graded gravel with silt
[h]Maximum dry unit weight
[i]Optimum water content.

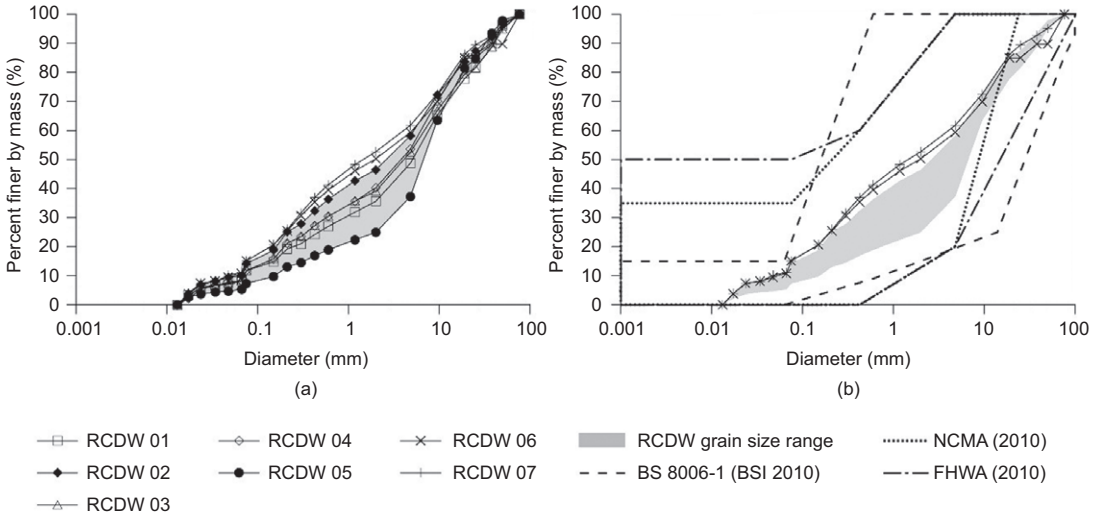

Figure 4. RCDW grain size distribution: (a) RCDW samples; (B) RCDW grain size distribution range and recommendations for backfill material – NCMA (2010), BS 8006-1 (BSI 2010) and FHWA (2010)

contents (see Table 1). The composition test reveals particle breakage after the compaction procedures performed during the second site plant filling: sample RCDW 07 presented more fine grains (particles smaller than 4.75 mm) compared with sample RCDW 06.

According to the Unified Soil Classification System (ASTM D 2487-06), the majority of RCDW samples are classified (Table 2) as poorly-graded sand with silt (GP-GM). The RCDW range is inside the recommended gradation of backfill materials for GRS structures (Figure 4b) as per FHWA (2010) and BS 8006-1 (BSI 2010). According to NCMA (2010), 7.8% of the RCDW range is outside their recommended gradation limits. Furthermore, all samples meet the recommendation of EBGEO (2011) for backfill materials in GRS structures. The grain size distribution range and non-plastic behaviour observed for RCDW enables it to be used as an alternative backfill material in GRS structures. Santos *et al*. (2010, 2013, 2014) and Vieira and Pereira (2015b, 2016) also verified the applicability of RCDW in this type of structure.

The standard Proctor compaction test results (Table 2) reveal mean values of maximum dry unit weight (γ_{d_max}) and optimum water content (w_{opt}) equal to 18.11 kN/m^3 and 14.6%, respectively. The dry unit weight results have shown a smaller variation (COV = 2.30%) compared to optimum water content results (COV = 8.41%). Sample RCDW 01 presented the highest value of $\gamma_{d\_máx}$, which can be attributed to its higher concrete content (Table 1). The variability of ceramic content can be pointed out as the factor responsible for the higher COV value of w_{opt}. It was noted that the w_{opt} value increases as the ceramic content decreases (the results for samples RCDW 01 and RCDW 07 validate this assumption). O'Mahony (1997), Poon and Chan (2006) and Cardoso *et al*. (2016) reported similar results.

The mean value of γ_{d_max} of the five samples initially tested (RCDW 01 to RCDW 05) were taken as a reference for calculating the degree of in-field compaction. Four vibratory roller (VR) passes performed on the bottom RCDW layer and six passes performed on the top RCDW layer provided a degree of soil compaction equal to 89% (Standard Proctor). An increase in vibratory roller passes did not influence the degree of soil compaction, as the RCDW water content was on the dry side of the compaction curve (water content equal to 9.92%, and COV equal to 9.49%). The eight passes of the vibratory hammer (VH) carried out on the top RCDW layer yielded a degree of soil compaction equal to 92% (water content of 7.16%, and COV = 5.14%). The results of the compaction process (the degree of soil compaction and water content) measured were higher than those observed by Santos *et al*. (2010, 2013, 2014) in the GRS structures built with RCDW.

4.2. Geogrids

4.2.1. *Tensile test in virgin samples and determination of confidence interval*

The results of tensile tests performed in five virgin specimens of each geogrid type (Figure 5) revealed smaller ultimate tensile strength ($\bar{T}_{ult\_v}$) compared to the manufacturer's information. For geogrid PVA-35, the strain at failure ($\bar{\varepsilon}_f$) was below 5% and inhibited the calculation of the secant tensile stiffness for a strain of 5% ($\bar{J}_{sec5}$). Geogrids PET-35 and PET-55 presented $\bar{\varepsilon}_f$ below 10%. The polyester (PET) geogrids exhibit $\bar{J}_{sec2}$ values higher than $\bar{J}_{sec5}$, associated with a bending of the load-strain curve between strains of 1% and 3% (Figure 5), typical in polyester geosynthetics. This behaviour is not significant in the tensile-strain curve of polyvinyl alcohol filament geogrids (PVA-35).

The geogrid load-strain curves (Figure 5) revealed a smaller variability of mechanical behaviour for geogrid PET-35 compared to the others. This result revealed smaller variability in the mechanical behaviour of the PET filament geogrids compared to that of the PVA filament geogrid. However, geogrid PET-55 presented higher variability for tensile strength values.

Based on virgin specimen mean values, the confidence intervals were determined as follows: firstly, once each value of t (Student's *t*-distribution random variable) corresponded to a specific confidence level, for each property, the confidence level value that contained all the test results from the five virgin specimens was fixed; thus, the maximum and minimum values of each virgin geogrid property were calculated and the range between them (maximum and minimum values) was, henceforward, called the 'confidence interval'. This procedure was adopted for each geogrid type (PVA-35, PET-35 and PET-55) and for each property evaluated (tensile strength, strain at failure and the tensile stiffness at 2% and 5% strain). Table 3 shows the mean values of the aforementioned properties and their respective coefficients of variation (COV) and confidence levels. It was observed that the confidence levels for those properties ranged from 96% to 98% for all geogrids.

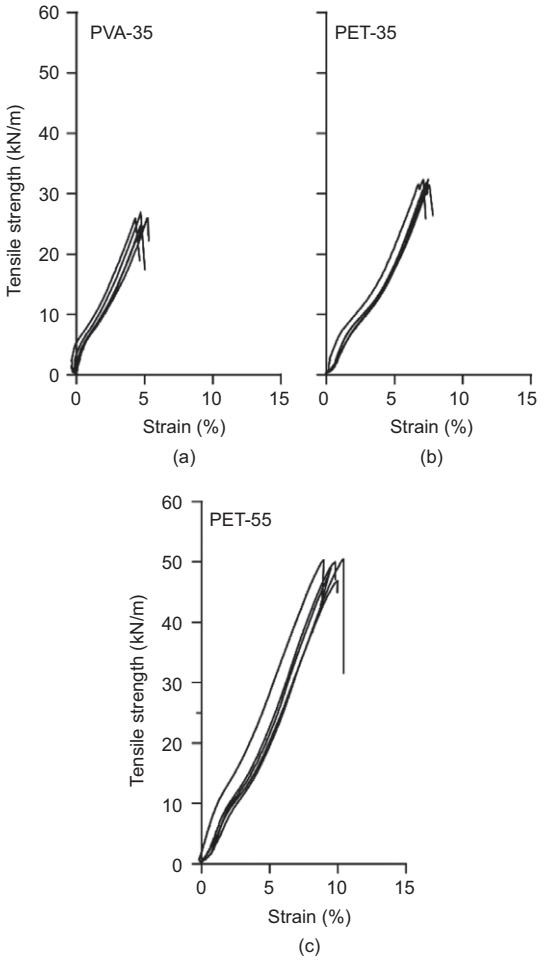

Figure 5. Tensile-strain curves of geogrid virgin samples tested

4.2.2. *Geogrids' tensile strength after installation damage*
After the installation damage, it can be assumed that a significant part of the investigated scenarios presented means value of damaged ultimate tensile strength ($\bar{T}_{ult\_d}$) smaller than the mean value of virgin ultimate tensile strength ($\bar{T}_{ult\_v}$). In the study, the percentages of reduction in $\bar{T}_{ult\_v}$ varied from 18.11% (PVA-35-H0-VH) to −6.01% (PET-35-H2*-NC). The negative values indicate ultimate tensile strength higher compared to $\bar{T}_{ult\_v}$. For all damaged scenarios investigated (except PVA-35-H2*-VR), the tensile strength results presented higher coefficient of variation (COV) values compared to the COV values of virgin specimens – similar results were reported by Paula *et al*. (2012) and Gonzalez-Torre *et al*. (2014). Table 4 summarises the mean and COV values of the tensile test results of virgin and damaged specimens.

For PVA-35 geogrid, the scenarios without compaction procedure (H0-NC, H1-NC, H2-NC and H2*-NC) revealed a similar reduction in the mean value of virgin ultimate tensile strength ($\bar{T}_{ult\_v}$) when considering both dropping heights (2.28% and 2.24% for 1.0 m and 2.0 m drop heights, respectively). The scenario with the protective layer (H2*-NC) induced more reduction in $\bar{T}_{ult\_v}$ (9.69%) compared to the scenario without the protection

Table 3. Results from tensile tests on virgin samples (5 specimens for each geogrid) associate with the Student's *t*-distribution analysis

	T_{max}	ε_f (%)	J_{sec2}	J_{sec5}
PVA-35				
Mean value	25.90 kN/m	4.83	548.98 kN/m	—
COV	2.89%	7.80	11.28%	—
Maximum value	27.00 kN/m	5.33	652.76 kN/m	—
Minimum value	24.80 kN/m	4.32	445.20 kN/m	—
Confidence level	97%	96	98%	—
PET-35				
Mean value	31.95 kN/m	7.35	410.67 kN/m	367.75 kN/m
COV	1.54%	2.10	11.13%	8.35%
Maximum value	32.61 kN/m	7.58	487.25 kN/m	419.18 kN/m
Minimum value	31.29 kN/m	7.12	334.09 kN/m	316.31 kN/m
Confidence level	96%	97	98%	98%
PET-55				
Mean value	49.93 kN/m	9.72	491.98 kN/m	449.12 kN/m
COV	3.06%	7.35	33.48%	15.48%
Maximum value	51.86 kN/m	10.52	668.69 kN/m	551.63 kN/m
Minimum value	46.80 kN/m	8.92	315.27 kN/m	346.61 kN/m
Confidence level	98%	97	98%	98%

Table 4. Mean values of tensile test results (five specimens) for virgin and damaged samples

Scenario	Geogrid		
	PVA-35	PET-35	PET-55
VS	25.90 (2.89)	31.95 (1.54)	49.33 (3.06)
H0-NC	25.81 (8.37)	32.61 (10.74)	47.39 (3.65)
H1-NC	25.31 (5.87)	31.63 (5.79)	50.29 (3.39)
H2-NC	25.32 (5.60)	28.86 (7.18)	47.72 (3.73)
H2*-NC	23.39 (10.30)	33.87 (10.49)	49.43 (4.75)
H0-VR	25.53 (6.99)	26.46 (10.43)	45.00 (5.56)
H1-VR	25.47 (11.43)	28.66 (8.12)	46.54 (5.82)
H2-VR	25.86 (6.05)	32.71 (10.40)	48.04 (6.17)
H2*-VR	23.38 (1.02)	31.20 (7.35)	47.56 (9.81)
H0-VH	21.21 (13.60)	26.31 (17.71)	49.33 (6.08)
H1-VH	24.42 (4.73)	28.72 (7.65)	42.51 (7.44)
H2-VH	22.91 (7.01)	29.19 (4.83)	44.55 (4.74)
H2*-VH	24.91 (9.59)	28.56 (5.39)	44.66 (6.33)

Note: Ultimate tensile strength in kN/m; Coefficient of variation (COV) are presented between parenthesis in percentage; VS, virgin specimens; H0, zero dropping height; H1, one-metre dropping height; H2, two-metre dropping height; H2*, two-metre dropping height over protection layer; NC, no compaction; VR, vibratory roller; VH, vibratory hammer.

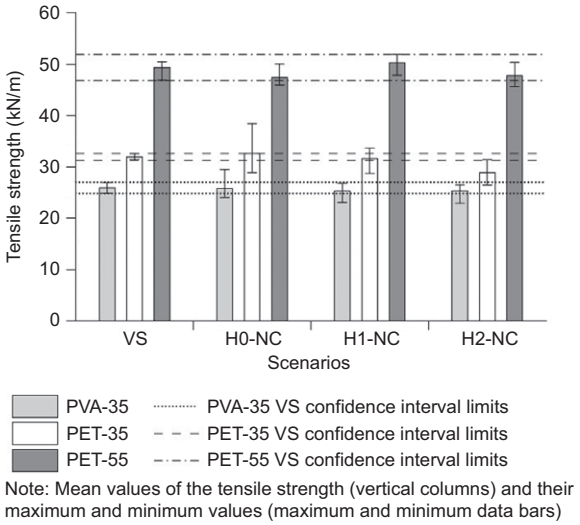

Figure 6. Geogrid tensile strength – effects of dropping process

layer (H2-NC; 2.24%). Where damage was caused exclusively by the compaction procedures (scenarios H0-VH and H0-VR), the vibratory hammer compaction caused a higher reduction in $\bar{T}_{ult\_v}$ (18.11%) than the vibratory roller compaction (1.43%). The cumulative effect of the dropping process and the vibratory roller compaction, scenarios H1-VR, H2-VR and H2*-VR, caused reductions in $\bar{T}_{ult\_v}$ equal to 1.66%, 0.15% and 9.73%, respectively. For the same geogrid, one can observe reductions equal to 5.71%, 11.54% and 3.82% for the scenarios that represent the synergy effect attached with the vibratory hammer compaction H1-VH, H2-VH and H2*-VH, respectively.

In the case of the PET-35 geogrid, scenarios H0-NC, H1-NC and H2-NC (without compaction procedures), show that as the drop height increased, the reduction in the mean value of virgin ultimate tensile strength ($\bar{T}_{ult\_v}$) also increased. The percentage of reduction in $\bar{T}_{ult\_v}$ is equal to 1.00% for 1.0 m drop height and 9.67% for 2.0 m drop height. For the analysed geogrid, the protective layer avoids the occurrence of damage since the reduction in $\bar{T}_{ult\_v}$ reduced from 9.67% (scenario H2-NC) to −6.01% (scenario H2*-NC). The scenarios that simulate the compaction process (H0-VH and H0-VR) show a similar reduction in $\bar{T}_{ult\_v}$: 17.65% for the vibratory hammer compaction and 17.18% for vibratory roller compaction. The analysed geogrid presented a reduction in $\bar{T}_{ult\_v}$ of 10.30%, −2.38% and 2.35% for the scenarios H1-VR, H2-VR and H2*-VR, respectively. The scenarios H1-VH, H2-VH and for H2*-VH exhibit a reduction in $\bar{T}_{ult\_v}$ of 10.11%, 8.64% and 10.61%, respectively.

For the PET-55 geogrid, the scenarios without a compaction procedure (H0-NC, H1-NC and H2-NC) revealed a slight increase (1.95%) in the mean value of virgin ultimate tensile strength ($\bar{T}_{ult\_v}$) for a 1.0 m dropping height and a similar reduction in $\bar{T}_{ult\_v}$ when it was submitted to a 0.0 m and 2.0 m dropping height (3.96% and 3.23%, respectively). Similar to the PET-35 geogrid, the protective layer avoids the occurrence of damage. The reduction in $\bar{T}_{ult\_v}$ decreased from 3.26% (scenario H2-NC) to −0.20% (scenario H2*-NC). The compaction procedures with the vibratory hammer (scenario H0-VH) did not cause any reduction or increase in the $\bar{T}_{ult\_v}$. However, the vibratory roller compaction (scenario H0-VR) caused a reduction in $\bar{T}_{ult\_v}$ equal to 8.78%. The cumulative effect of the dropping process attached with the vibratory hammer compaction caused a higher reduction in $\bar{T}_{ult\_v}$ (H1-VH = 13.83%, H2-VH = 9.69% and H2*-VH = 9.47%) compared with the synergy involving the vibratory roller compaction (H1-VR = 5.66%, H2-VR = 2.62% and H2*-VR = 3.59%).

The scenarios without a compaction procedure (H0-NC, H1-NC and H2-NC) help to identify the influence of the dropping process on the installation damage to geogrids (Figure 6). It affected the three studied geogrids in different ways. Results have shown that the increase in the dropping height of RCDW cannot be directly associated with an increase in installation damage. The damage caused by 0.0 m and 1.0 m dropping heights does not seem to be correlated with the geogrid characteristics. However, the damage caused by the 2.0 m dropping height seems to become more severe as the geogrids' tensile stiffness decreases. It was observed that PVA-35 geogrid presented more resistance to the 2.0 m dropping height when compared to PET-35. Bearing in mind a possible influence of the polymer type (PET-35 and PET-55 geogrids), the dropping process caused more damage to the geogrid with the smallest mass per unit area (PET-35, $M_A = 185$ g/m^2). However, it is important to keep in mind that geogrids with different geometries and element structures can present the same value of mass per unit area but different installation damage levels.

The RCDW protection layer (scenarios H2*-NC) proved to be efficient for PET geogrids since its presence avoided the reduction in the mean value of virgin ultimate tensile strength ($\bar{T}_{ult\_v}$) compared to the scenario without

the protection layer (scenario H2-NC). However, the PVA-35 geogrid exhibits the opposite behaviour: the reduction in $\bar{T}_{ult\_v}$ increased with the protection layer. These results can be associated with the particle shapes of the material used as a protection layer (in this case, RCDW). Given that RCDW contains gravel particles, if a pointed particle stays in contact with the geogrid after the protection layer is arranged, it could concentrate the impact caused by the dropping process. Based on that, using a protection layer constructed with fine RCDW might reduce installation damage. Furthermore, the difference in the efficiency of the protection layer against installation damage related to the dropping height can also be associated with the geogrid's flexibility. In the case of more flexible ribs, the energy caused by the impact could be better distributed. Further investigations must be performed to validate the assumption mentioned above. Figure 7 shows the protection layer influences on the geogrids' ultimate tensile strength.

The scenario with a 0.0 m dropping height and different compaction methods (H0-VR and H0-VH) led to the assessment of the influence of the latter (Figure 8). Using vibratory roller compaction revealed that the PVA yarn geogrid exhibited higher resistance (virgin specimens with $\bar{J}_{sec2} = 548$ kN/m) than the PET yarn geogrids (virgin specimens with $\bar{J}_{sec2} = 410$ kN/m), which can be an indication that, considering this compaction method, the increase in the damage is inversely related to tensile stiffness. Using vibratory hammer compaction indicated that the geogrid with higher ultimate tensile strength value (PET-55) presented higher resistance to damage than that with the lowest strength value (PET-35). The higher coefficient of variation (COV) values caused by the vibratory hammer compaction compared with those of the vibratory roller shows geogrid susceptibility to the vibratory hammer compaction method. The higher degree of soil compaction obtained with the vibratory hammer compaction (92%) compared with the vibratory roller (89%) is responsible for this result.

It must be highlighted that the reductions in the mean value of virgin ultimate tensile strength ($\bar{T}_{ult\_v}$) caused by the compaction procedure were higher than those caused by the dropping process. The same is applicable to the COV obtained from tensile tests. Thus, compared to the dropping process, the compaction procedure results presented higher changes in tensile strength behaviour of individual samples.

Considering the synergy effect of the dropping process and the compaction procedures, for both PET geogrids, the scenarios with a 1.0 m dropping height (H1-VH and H1-VR) caused a higher reduction in the mean value of virgin ultimate tensile strength ($\bar{T}_{ult\_v}$) than the scenarios with a 2.0 m dropping height (H2-VH and H2-VR). For all geogrids investigated, the scenarios with vibratory hammer compaction (H1-VH, H2-VH and H2*-VH) caused higher reductions in the $\bar{T}_{ult\_v}$ compared to the scenarios involving the vibratory roller compaction (H1-VR, H2-VR and H2*-VR). The higher degree of soil compaction obtained with the vibratory hammer compaction is also identified as being responsible for this result. Figures 9 and 10 present the results of tensile strength related to the vibratory roller and vibratory hammer compaction methods, respectively.

These synergy effects show that the correlation between the dropping process and compaction method involve aspects of a complex mechanism related to the filling material (variability, dropping height, particle arrangement and compaction effects) and the reinforcing material (yarn polymer, open area, mass per unit area, tensile and bending stiffness). Huang (2006) also reported the difficulty of obtaining a correlation between the reduction factors and different compaction conditions for gravel materials.

Based on the virgin sample confidence interval for tensile strength (obtained from the Student's *t*-distribution – Table 3) and the ultimate tensile strength mean values for damaged samples (Table 4), the reduction factors related to the tensile strength (RF_{T_ult}) were calculated and are shown in Table 5. The RF_{T_ult} varied

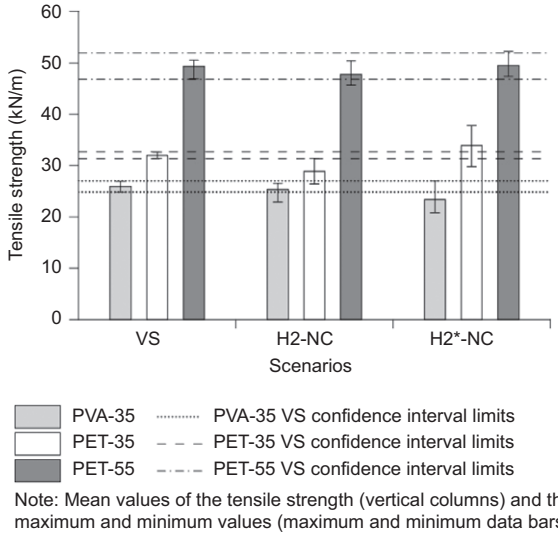

Figure 7. Geogrid tensile strength – influences of protection layer

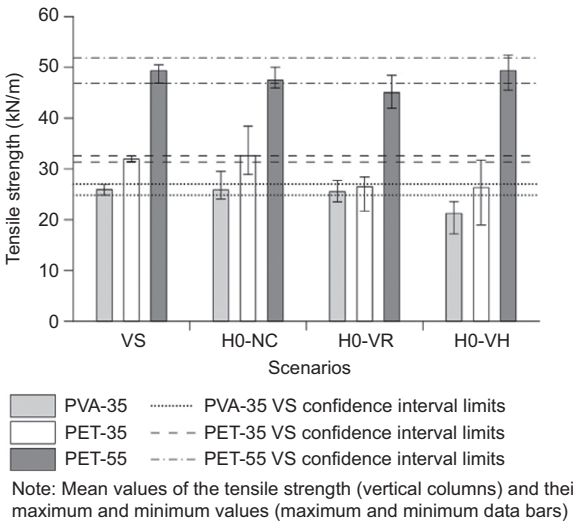

Figure 8. Geogrid tensile strength – effects of compaction method

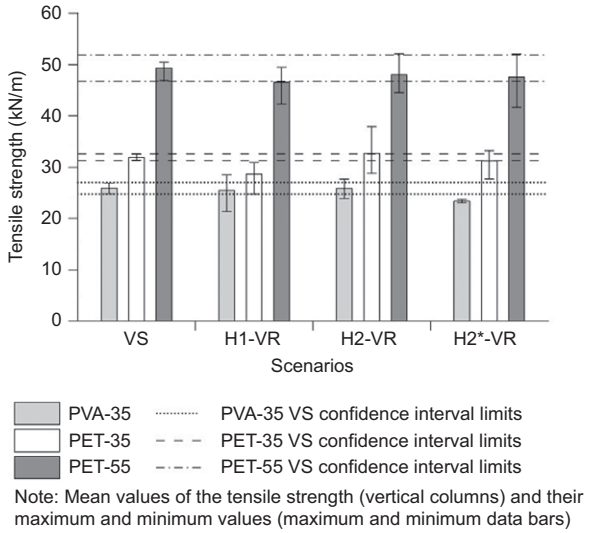

Note: Mean values of the tensile strength (vertical columns) and their maximum and minimum values (maximum and minimum data bars)

Figure 9. Geogrid tensile strength – effects of vibratory roller compaction method

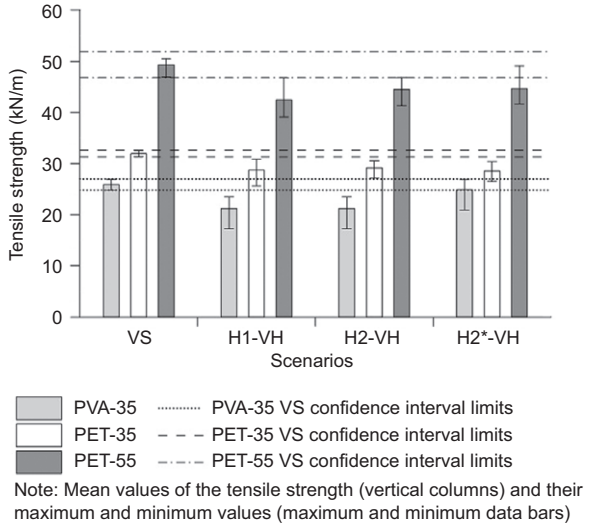

Note: Mean values of the tensile strength (vertical columns) and their maximum and minimum values (maximum and minimum data bars)

Figure 10. Geogrid tensile strength – effects of vibratory hammer compaction method

from 0.94 (PET-55-H2*-NC) to 1.22 (PVA-35-H0-VH). The range of installation damage reduction factors presented is smaller than those recommended by FHWA (2010).

Table 5 shows scenarios with reduction factors smaller than 1.00. Allen and Bathurst (1994) attributed these phenomena to a geogrid strain hardening caused by the stresses developed during the compaction procedures. Paula *et al*. (2004) and Huang and Chiou (2006) associated reduction factors smaller than 1.00 with a rearrangement of geosynthetic fibers. Furthermore, Kondo *et al*. (1992) and Rowe *et al*. (2009) recorded the influence of the specimen condition (storage and temperature) in tensile tests results. Since no tests were performed to verify these correlations, the authors highlight that reduction factors lower than the unit should not be considered in the design, therefore it is recommended that RF_{T_ult} equal to 1.00 be adopted for these scenarios. The presence of scenarios

Table 5. Reduction factors related to the ultimate tensile strength for all scenarios

Scenario	PVA-35	PET-35	PET-55
H0-NC	1.00	1.00	1.00
H1-NC	1.00	1.11	1.00
H2-NC	1.11	0.94[a]	1.00
H2*-NC	1.00	1.21	1.10
H0-VR	1.00	1.12	1.06
H1-VR	1.00	0.98[a]	1.00
H2-VR	1.11	1.02	1.00
H2*-VR	1.22	1.21	1.00
H0-VH	1.06	1.11	1.16
H1-VH	1.13	1.09	1.11
H2-VH	1.00	1.12	1.10
H2*-VH	1.00	1.00	1.00

Note: H0, zero dropping height; H1, one-metre dropping height; H2, two-metre dropping height; H2*, two-metre dropping height over protection layer; NC, no compaction; VR, vibratory roller; VH, vibratory hammer.
[a]The adoption of a reduction factor equal to 1.00 is recommended.

with RF_{T_ult} equal to 1.00, different from the major reduction factors reported by the literature ($RF_{ID} > 1.00$), is also clear. Given that this study adopted the Student's *t*-distribution for statistical analysis, RF_{T_ult} greater than 1.00 confers more reliability to affirm that installation damage caused.

Considering the synergy effect of the dropping height and compaction method, the values of RF_{T_ult} presented in Table 5 for scenarios H1-VR, H2-VR, H2*-VR, H1-VH, H2-VH and H2*-VH do not show a direct relationship. In general, the multiplication of independent reduction factors – one related to the dropping height and another to the compaction method – would lead to higher RF_{T_ult} than those obtained from the in-field test facility simulations. Although the process of multiplying independent reduction factors acts on behalf of safety for engineering projects using geosynthetics, this process does not lead to an investigation into the complex mechanism of installation damage that happens when constructing GRS structures.

As previously mentioned, the damaged scenarios exhibited coefficients of variation (COV) higher than those calculated for the virgin sample, resulting in minimum (or even maximum) values outside the confidence interval of the virgin samples. These conditions illustrate the importance of considering a statistical analysis for calculating the reduction factor due to installation damage. Moreover, despite the reduction factors caused by the dropping height having exhibited values equal to 1.00 (in the majority), it is clear that the dropping process affects the individual behaviour of the geogrid samples.

4.2.3. *Geogrids' strain at failure and secant tensile stiffness after installation damage*

Allen and Bathurst (1994) emphasised the importance of strain monitoring to assess the evolution of geogrid tensile strength. Generally, the strain at failure of PET geogrids (PET-35 and PET-55) presented higher modifications

than those of the PVA-35 geogrid for both investigated factors (dropping height and compaction method). The results revealed that the increase in the dropping height reduced the strain at failure of the PET geogrids tested, and compaction with the vibratory hammer caused higher reduction in the strain at failure than vibratory roller compaction for all geogrids tested. In terms of reduction factors (Table 6), PVA-35 geogrid exhibited RF_{ε_f} equal to 1.00 for all scenarios evaluated. For geogrid PET-35, only scenarios H2-NC, H0-VR, H1-VH, H2-VH and H2*-VH resulted in RF_{ε_f} higher than 1.00. Geogrid PET-55 presented a narrow interval of RF_{ε_f} values – from 1.04 to 1.10 – for scenarios H2-NC, H2-VH and H0-VH.

According to Paula *et al.* (2004) and Huang and Liao (2007), the secant tensile stiffness assessment is highly indicated in evaluating the performance of polymeric materials. Therefore, PET geogrids exhibited excellent results (Table 7), given that they did not suffer modification in the values of $J_{sec\,2}$ and J_{sec5}, resulting in a reduction factor equal to 1.00 in this regard (Table 8). PVA-35 geogrid, for all scenarios with vibratory hammer compaction and with a protective cover layer, presented values of $RF_{J\,sec\,2}$ equal to 1.25 or higher (Table 8). The secant tensile stiffness of the PVA geogrid seems to be more sensitive to damage than that of the PET geogrids tested.

The strain at failure (ε_f) and secant tensile stiffness at 2% and 5% strains (J_{sec2} and J_{sec5}, respectively) seem to be less affected by the installation damage than the ultimate tensile strength (T_{ult}), which is in accordance with results reported by Allen and Bathurst (1994) and Gonzalez-Torre *et al.* (2014). Most of the scenarios (all of the PET geogrids and six related to PVA geogrid) exhibited a reduction factor equal to 1.00 (Tables 6 and 8). As previously mentioned, this study used a statistical analysis to validate the occurrence of damage. However, the high coefficients of variation (COV) observed for virgin geogrid sample strains at failure and secant tensile stiffness (Table 8) indicate that the virgin sample parameter confidence intervals are too broad. Thus, the mean damaged value has to be very low or very high – compared to the virgin sample mean value – to exhibit reduction factors different from 1.00.

One must bear in mind that the method of monitoring the strain during the tensile strength test can be a reason for the wide range of secant tensile stiffness values obtained. The monitoring occurs in only one longitudinal rib and the rupture does not occur in all ribs tested simultaneously (the prevailing condition in the wide strip tensile test). Therefore, strain measurement can be affected by the sequence of ruptures in different ribs and its influence on the monitored one. Using digital image correlation together with short-range photogrammetry may provide more reliable strain measurement results.

Table 6. Reduction factors related to the strain at failure for all scenarios

Scenario	PVA-35	PET-35	PET-55
H0-NC	1.00	1.00	0.93[a]
H1-NC	1.00	1.00	1.00
H2-NC	1.00	1.14	1.04
H2*-NC	1.00	1.00	0.89[a]
H0-VR	1.00	1.13	1.00
H1-VR	1.00	1.00	0.94[a]
H2-VR	1.00	1.00	0.93[a]
H2*-VR	1.00	1.00	0.96[a]
H0-VH	1.00	1.00	1.10
H1-VH	1.00	1.23	1.00
H2-VH	1.00	1.15	1.04
H2*-VH	1.00	1.15	1.00

Note: H0, zero dropping height; H1, one-metre dropping height; H2, two-metre dropping height; H2*, two-metre dropping height over protection layer; NC, no compaction; VR, vibratory roller; VH, vibratory hammer.
[a]The adoption of a reduction factor equal to 1.00 is recommended.

Table 7. Secant tensile stiffness mean values and coefficient of variation obtained from tensile tests on virgin and damaged specimens

Scenarios	PVA-35	PET-35		PET-55	
	J_{sec2}	J_{sec2}	J_{sec5}	J_{sec2}	J_{sec5}
VS	548.98 (11.28)	410.67 (11.13)	367.75 (8.35)	491.98 (21.43)	449.12 (13.62)
H0-NC	636.44 (9.90)	410.32 (14.43)	360.57 (11.03)	524.66 (5.40)	466.56 (5.81)
H1-NC	560.29 (11.62)	431.67 (13.74)	381.98 (16.42)	616.08 (12.52)	544.01 (10.03)
H2-NC	559.56 (28.06)	481.60 (21.93)	364.89 (20.58)	598.23 (6.56)	529.84 (4.50)
H2*-NC	415.93 (19.19)	417.31 (9.92)	351.45 (9.20)	549.20 (5.30)	496.47 (2.34)
H0-VR	475.00 (18.91)	345.75 (11.24)	307.41 (8.44)	512.82 (5.49)	474.15 (2.85)
H1-VR	582.19 (12.14)	357.67 (24.96)	322.21 (19.58)	494.87 (2.76)	446.39 (4.270
H2-VR	449.92 (10.65)	420.10 (6.64)	362.47 (4.11)	470.95 (23.12)	441.28 (16.27)
H2*-VR	428.09 (10.57)	408.62 (4.92)	348.71 (4.26)	525.34 (11.56)	471.77 (8.35)
H0-VH	435.86 (15.77)	433.27 (16.97)	357.61 (11.21)	484.04 (19.97)	454.04 (11.21)
H1-VH	548.98 (11.28)	392.69 (16.54)	340.43 (13.57)	540.51 (29.97)	498.91 (19.24)
H2-VH	636.44 (9.90)	458.27 (21.55)	382.03 (16.41)	529.04 (10.97)	483.84 (7.95)
H2*-VH	560.29 (11.62)	388.00 (6.19)	339.24 (7.30)	554.00 (7.62)	491.43 (3.15)

Note: Values of J_{sec2} and J_{sec2} are presented in kN/m; Coefficient of variation (COV) are presented between parenthesis in percentage; VS, virgin specimens; H0, zero dropping height; H1, one metre-dropping height; H2, two-metre dropping height; H2*, two-metre dropping height over protection layer; NC, no compaction; VR, vibratory roller; VH, vibratory hammer.

Table 8. Reduction factors related to the tensile stiffness with 2% and 5% strain for all scenarios

Scenarios	PVA-35	PET-35		PET-55	
	RF_{J_sec2}	RF_{J_sec2}	RF_{J_sec5}	RF_{J_sec2}	RF_{J_sec5}
H0-NC	1.00	1.00	1.00	1.00	1.00
H1-NC	1.00	1.00	1.00	1.00	1.00
H2-NC	1.00	1.00	1.00	1.00	1.00
H2*-NC	1.32	1.00	1.00	1.00	1.00
H0-VR	1.00	1.00	1.00	1.00	1.00
H1-VR	1.00	1.00	1.00	1.00	1.00
H2-VR	1.00	1.00	1.00	1.00	1.00
H2*-VR	1.28	1.00	1.00	1.00	1.00
H0-VH	1.26	1.00	1.00	1.00	1.00
H1-VH	1.27	1.00	1.00	1.00	1.00
H2-VH	1.27	1.00	1.00	1.00	1.00
H2*-VH	1.25	1.00	1.00	1.00	1.00

Note: H0, zero dropping height; H1, one-metre dropping height; H2, two-metre dropping height; H2*, two-metre dropping height over protection layer; NC, no compaction; VR, vibratory roller; VH, vibratory hammer.

5. CONCLUSIONS

This paper reported on installation damage to geogrids caused by recycled construction and demolition waste (RCDW). An in-field test facility was constructed to reproduce the conditions of construction (dropping process and compaction procedures) of a geosynthetic-reinforced soil structure (GRS) using RCDW as backfill material. Tensile tests were carried out in damaged geogrid specimens and the main conclusions obtained are presented below.

(1) The variability of the geotechnical characteristics of RCDW is clear, but they do not prevent the application of this non-conventional material as backfill material in GRS structures. After an adequate characterisation before its application, the adoption of a grain size distribution range is strongly suggested when evaluating the gradation limits recommended by technical standards.
(2) Dropping processes at different heights (0.0 m, 1.0 m and 2.0 m) caused slight reductions in the ultimate tensile strength of geogrids. The increase in the dropping height showed no direct association with the increase in damage. However, despite this finding, the authors strongly advise an in-field investigation when diverse dropping heights are present in the practice of geosynthetic reinforced soil construction. The use of a protective layer comprising RCDW to avoid the damage caused by the dropping process is controversial. The RCDW particle shapes and position (close to the geogrid rib) can be identified as a factor related to the increase in damage. Thus, the adoption of fine grain RCDW can be seen as an attractive alternative to reduce the damage caused by the dropping process.
(3) Compaction methods were revealed to be a relevant factor for geogrid installation damage caused by RCDW. It was observed that damage caused by the compaction methods was higher than that caused by the dropping processes. In general, the vibratory hammer compaction promoted the highest reduction in the geogrids' ultimate tensile strength because of the higher degree of soil compaction reached in comparison with the vibratory roller compaction.
(4) Considering the cumulative effect of the dropping process and compaction procedures, most of the scenarios evaluated indicate that the multiplication of an individual reduction factor would be conservative compared to the synergy effect. Although this procedure acts on behalf of safety for engineering projects using geosynthetics, it impairs a better understanding of the complexity of the synergic effects involved in geogrid mechanical damage and prevents the adoption of reduction factors strictly related to particular cases (dropping height, compaction method, etc), which could be more reliable.

Based on these conclusions, this paper confirms the importance of obtaining reduction factors for specific situations when RCDW is used as a backfill material in GRS. The results highlight the complexity of mechanisms related to the generation of installation damage and contribute to a better understanding of the processes involved in mechanical damage. The values of RF presented encourage the design and construction of GRS structures with RCDW, an interesting option to fulfil the technical and economic aspects required by these structures associated with environmental concerns.

ACKNOWLEDGEMENTS

The authors would like to thank the Federal University of Goiás (UFG), National Council for Scientific and Technological Development (CNPq), Brazilian Ministry of Education (CAPES), RENOVE Waste Management, Huesker Geosynthetics, MOLD Precast Structures, SETE Engineering, Terra and Entulho, Terra Móvel, Global Leasing, REISFORT's and the University of São Paulo for the support provided to the research activities reported in this paper.

NOTATION

Basic SI units are given in parentheses.

COV	coefficient of variation (dimensionless)
d	particle diameter (m)
G_s	specific gravity (dimensionless)
$\bar{J}_{sec}$	secant tensile stiffness mean value (kN/m)
$\bar{J}_{sec2}$	secant tensile stiffness at 2% strain mean value (kN/m)
$\bar{J}_{sec5}$	secant tensile stiffness at 5% strain mean value (kN/m)
M_A	mass per unit area (kg/m^2)
n	sample size (dimensionless)
PI	plasticity index (dimensionless)
RF	global reduction factor (dimensionless)
RF_{CR}	creep reduction factor (dimensionless)
RF_D	durability reduction factor (dimensionless)
RF_{ID}	reduction factor related to installation damage (dimensionless)
RF_{J_sec2}	reduction factor related to the secant tensile stiffness at 2% strain (dimensionless)
RF_{J_sec5}	reduction factor related to the secant tensile stiffness at 5% strain (dimensionless)
RF_{T_ult}	reduction factor related to the ultimate tensile strength (dimensionless)
RF_X	reduction factor related to the X parameter (dimensionless)
RF_{ε_f}	reduction factor related to the strain at failure (dimensionless)
s	sample standard deviation (parameter dependent)
T_{al}	geosynthetic allowable strength (N/m)
$\bar{T}_{ult}$	ultimate tensile strength mean value (kN/m)
$\bar{T}_{ult\_d}$	ultimate tensile strength mean value from damaged specimens (kN/m)
$\bar{T}_{ult\_v}$	ultimate tensile strength mean value from virgin specimens (kN/m)
t	Student's t-distribution random variable (dimensionless)
w_{opt}	optimum water content (%)
$\bar{X}$	virgin sample mean value of the analysed parameter (parameter dependent)
$\bar{X}_d$	mean value of the analysed parameter from damaged specimens (parameter dependent)
x	sample mean value (parameter dependent)
γ_{d_max}	maximum dry unit weight (kN/m^3)
$\bar{\varepsilon}_f$	strain or elongation at failure mean value (%)
μ	population mean (parameter dependent)

ABBREVIATIONS

CDW	construction and demolition waste
GP-GM	poorly-graded sand with silt
GRS	geosynthetic reinforced soils
GW-GM	well-graded gravel with silt
H0	zero-metre dropping height
H1	one-metre dropping height
H2	two-metre dropping height
H2*	two-metre dropping height over protection layer
MD	machine direction
NBR	Brazilian standards
NC	no compaction
NP	non-plastic behaviour
PET	polyester
PET-35	geogrid with polyester filaments and 35 kN/m tensile strength
PET-55	geogrid with polyester filaments and 55 kN/m tensile strength
PVA	polyvinyl alcohol
PVA-35	geogrid with polyvinyl alcohol filaments and 35 kN/m tensile strength
RCDW	recycled construction and demolition waste
RCDW 01	RCDW sample number one
RCDW 02	RCDW sample number two
RCDW 03	RCDW sample number three
RCDW 04	RCDW sample number four
RCDW 05	RCDW sample number five
RCDW 06	RCDW sample number six
RCDW 07	RCDW sample number seven
SP-SM	poorly-graded gravel with silt
USCS	Unified Soil Classification System
VH	vibratory hammer
V-M ratio	ratio of coating volume to the mass of yarns
VR	vibratory roller
VS	virgin sample

REFERENCES

ABRECON (Brazilian Association for the Recycling of Construction and Demolition Wastes) (2017). Sectorial Research Report 2014/2015. 2015. See https://issuu.com/sanchocom/docs/relatorio-pesq2015_abrecon?embed_cta=read_more&embed_context=embed&embed_domain=abrecon.org.br&embed_id=6666802%2F37960095 (accessed 19/12/2017) (in Portuguese).

Allen, T. M. & Bathurst, R. J. (1994). Characterization of geosynthetic load-strain behavior after installation damage. *Geosynthetics International*, **1**, No. 2, 181–199.

Allen, T. M. & Bathurst, R. J. (1996). Combined allowable strength reduction factor for geosynthetic creep and installation damage. *Geosynthetics International*, **3**, No. 3, 407–439.

Arulrajah, A., Rahman, M. A., Piratheepan, J., Bo, M. W. & Imteaz, M. A. (2014). Evaluation of interface shear strength properties of geogrid-reinforced construction and demolition materials using a modified large scale direct shear testing apparatus. *Journal of Materials in Civil Engineering*, **26**, No. 5, 974–982.

ASTM D 2487-06 *Standard Practice for Classification of Soils for Engineering Purposes (Unified Soil Classification System)*. ASTM International, West Conshohocken, PA, USA.

ASTM D 6637-15 *Standard Test Method for Determining Tensile Properties of Geogrids by the Single or Multi-Rib Tensile Method*. ASTM International, West Conshohocken, PA, USA.

Austin, R. (1997). The effect of installation activities and fire exposure on geogrid performance. *Geotextiles and Geomembranes*, **15**, No. 4–6, 367–376.

Barbosa, F. A. S. & Santos, E. C. G. (2013). Geogrid mechanical damages due to recycled construction and demolition wastes. *Proceedings of the 14th International Waste Management and Landfill Symposium*, Cossu R., He P., Kjeldsen P., Matsufuji Y.,

Reinhart D. & Stegmann, R., Editors, International Waste Working Group (IWWG), Cagliari, Sardegna, Italy, pp. 1–8.

Barbosa, F. A. S., Silva, E. M. & Santos, E. C. G. (2016). Polypropylene (PP) geosynthetics strength reduction due installation damages caused by construction and demolition waste (RCDW). *Proceedings of the 16th Brazilian Conference of Soils Mechanics and Geotechnical Engineering*, Simões G. F. & Pimenta de Ávila J., Editors, Brazilian Association of Soil Mechanics and Geotechnical Engineering (ABMS), Belo Horizonte, Minas Gerais, Brazil, pp. 1–6.

Basu, D., Misra, A. & Puppala, A. J. (2014). Sustainability and geotechnical engineering: perspectives and review. *Canadian Geotechnical Journal*, **52**, No. 1, 96–113.

Bathurst, R. J. & Miyata, Y. (2015). Reliability-based analysis of combined installation damage and creep for the tensile rupture limit state of geogrid reinforcement in Japan. *Soils and Foundations*, **55**, No. 2, 437–446.

Bathurst, R. J., Huang, B. & Allen, T. M. (2011). Analysis of installation damage tests for LRFD calibration of reinforced soil structures. *Geotextiles and Geomembranes*, **29**, No. 3, 323–334.

Bathurst, R. J., Huang, B. Q. & Allen, T. M. (2012). Interpretation of laboratory creep testing for reliability-based analysis and load and resistance factor design (LRFD) calibration. *Geosynthetics International*, **19**, No. 1, 39–53.

Brito, J., Pereira, A. S. & Correia, J. R. (2005). Mechanical behaviour of non-structural concrete made with recycled ceramic aggregates. *Cement and Concrete Composites*, **27**, No. 4, 429–433.

BSI (2007). *EN ISO 10722:2007: Geosynthetics, index test procedure for the evaluation of mechanical damage under repeated loading – damage caused by granular material*. BSI, London, UK.

BSI (2010). *8006-1: Code of Practice for Strengthened/Reinforced Soils and Other Fills*. BSI, London, UK.

Cardoso, R., Silva, R. V., Brito, J. & Dhir, R. (2016). Use of recycled aggregates from construction and demolition waste in geotechnical applications: a literature review. *Waste Management*, **49**, 131–145.

Cho, S. D., Lee, K. W., Cazzuffi, D. A. & Jeon, H. Y. (2006). Evaluation of combination effects of installation damage and creep behavior on long-term design strength of geogrids. *Polymer Testing*, **25**, No. 6, 819–828.

Correia, A. G., Winter, M. G. & Puppala, A. J. (2016). A review of sustainable in transport infrastructure geotechnics. *Transportation Geotechnics*, **7**, 21–28.

Damians, I. P., Bathurst, R. J., Adroguer, E. A., Josa, A. & Lloret, A. (2017). Environmental assessment of earth retaining wall structures. *Environmental Geotechnics*, **4**, No. 6, 415–431.

Damians, I. P., Bathurst, R. J., Adroguer, E. A., Josa, A. & Lloret, A. (2018). Sustainability assessment of earth-retaining wall structures. *Environmental Geotechnics*, **5**, No. 4, 187–203.

EBGEO (2011). *Recommendations for Design and Analysis of Earth Structures Using Geosynthetic Reinforcements – EBGEO*. German Geotechnical Society: Ernst and Sohn GmbH & Co. KG, Berlin, Germany.

FHWA (Federal Highway Administration) (2010). *Design and construction of mechanically stabilized earth walls and reinforced soil slopes*, Berg, R. R., Christopher, B. R. & Samtani, N. C., Editors, FHWA-NHI-10-024. FHWA's report, FHWA, Washington, DC, USA.

Gonzalez-Torre, I., Calzada-Perez, M. A., Vega-Zamanillo, A. & Castro-Fresno, D. (2014). Damage evaluation during installation of geosynthetics used in asphalt pavements. *Geosynthetics International*, **21**, No. 6, 377–386.

Herrador, R., Perez, P., Garach, L. & Ordonez, J. (2012). Use of recycled construction and demolition waste aggregate for road course surfacing. *Journal of Transportation Engineering*, **138**, No. 2, 182–190.

Hsieh, C. & Wu, J. (2001). Installation survivability of flexible geogrids in various pavement subgrade materials. *Transportation Research Record*, **1772**, 190–196.

Huang, C. C. (2006). Laboratory simulation of installation damage of a geogrid. *Geosynthetics International*, **13**, No. 3, 120–132.

Huang, C. C. & Chiou, S. L. (2006). Investigation of installation damage of some geogrids using laboratory tests. *Geosynthetics International*, **13**, No. 1, 23–35.

Huang, C. C. & Liao, C. C. (2007). Abrasion damage of geogrids induced by turbid flow. *Geotextiles and Geomembranes*, **25**, No. 2, 128–138.

Huang, C. C. & Wang, Z. N. (2007). Installation damage of geogrids: influence of load intensity. *Geosynthetics International*, **14**, No. 2, 65–75.

Hufenus, R., Ruegget, R. & Flum, D. (2002). Geosynthetics for reinforcement – resistance to damage during installation. *Proceedings of the 7th International Conference on Geosynthetics* (Cazzuffi D., Greenwood J., HEibaum M., Leshchinsky D. & Tatsuoka F., Editors, International Geosynthetics Society (IGS), Nice, France, vol. 2, pp. 1387–1390.

Hufenus, R., Rüegger, R., Flum, D. & Sterba, I. (2005). Strength reduction factors due to installation damage of reinforcing geosynthetics. *Geotextiles and Geomembranes*, **23**, No. 5, 401–424.

Jeon, H. Y. & Bouazza, A. (2010). Experimental investigation of installation damage for geogrids. *Proceedings of the Institution of Civil Engineers – Ground Improvement*, **163**, No. 4, 197–205.

Koerner, G. R. & Koerner, R. M. (1990). The installation survivability of geotextiles and geogrids. *Proceedings of the 4th International Conference on Geotextiles, Geomembranes, and Related Products*, Den Hoedt G., Editors, Taylor & Francis Group, The Hague, South Holland, the Netherlands, pp. 597–602.

Kondo, H., Tanala, T., Masuda, T. & Nakajima, A. (1992). Aging effects in 16 years on mechanical properties of commercial polymers. *Pure and Applied Chemistry*, **64**, No. 12, 1945–1958.

Leite, F. C., Motta, R. S., Vasconselos, K. L. & Bernucci, L. (2011). Laboratory evaluation of recycled construction and demolition waste for pavements. *Construction and Building Materials*, **25**, No. 6, 2972–2979.

Lim, S. Y. & McCartney, J. S. (2013). Evaluation of effect of backfill particle size on installation damage reduction factors for geogrids. *Geosynthetics International*, **20**, No. 2, 62–72.

Miyata, Y. & Bathurst, R. J. (2015). Reliability analysis of geogrid installation damage test data in Japan. *Soils and Foundations*, **55**, No. 2, 393–403.

Nagataki, S., Gokce, A., Saeki, T. & Hisada, M. (2004). Assessment of recycling process induced damage sensitivity of recycled concrete aggregates. *Cement and Concrete Research*, **34**, No. 6, 965–971.

NCMA (National Concrete Masonry Association) (2010). *Design Manual for Segmental Retaining Walls*, 3rd edn, NCMA, Herndon, VA, USA.

Niekerk, A. A. V., Molenaar, A. A. A. & Houben, L. J. M. (2002). Effect of material quality and compaction on the mechanical behavior of base course materials and pavement performance. *Proceedings of the 6th International Conference on the Bearing Capacity of Roads and Airfields*, Correia, A. G. & Branco, F. E., Editors, Balkema, Lisbon, Portugal, pp. 1071–1079.

O'Mahony, M. M. (1997). An analysis of the shear strength of recycled aggregates. *Materials and Structures*, **30**, No. 10, 599–606.

Ossa, A., Garciá, J. L. & Botero, E. (2016). Use of recycled construction and demolition waste (CDW) aggregates: a sustainable alternative for pavement construction industry. *Journal of Cleaner Production*, **135**, 379–386.

Paula, A. M., Pinho-Lopes, M. & Lopes, M. L. (2004). Damage during installation laboratory test. Influence of the type of granular material. *Proceedings of the 3rd European Geosynthetics Conference*, Munich, Germany, Zentrum Geotechnik, Munich, Germany, pp. 603–606.

Paula, A. M., Pinho-Lopes, M. & Lopes, M. L. (2012). Effect of damage during installation on the mechanical behaviour of biaxial woven polyester geogrid. *Proceedings of the 5th European Geosynthetic Congress*, Leiro A., Editor, International Geosynthetic Society, Valencia, Spain, pp. 446–451.

Pinho-Lopes, M. & Lopes, M. L. (2014). Tensile properties of geosynthetics after installation damage. *Environmental Geotechnics*, **1**, No. 3, 161–178.

Pinho-Lopes, M., Paula, A. M. & Lopes, M. L. (2018). Long-term response and design of two geosynthetics: effect of field installation damage. *Geosynthetics International*, **25**, No. 1, 98–117.

Poon, C. S. & Chan, D. (2006). Feasible use of recycled concrete aggregates and crushed clay brick as unbound road sub-base. *Construction and Building Materials*, **20**, No. 8, 578–585.

Richardson, G. (1998). Field evaluation of geosynthetic survivability in aggregate road base. *Geotechnical Fabrics Report*, **16**, No. 7, 34–38.

Rosete, A., Lopes, P. M., Pinho-Lopes, M. & Lopes, M. L. (2013). Tensile and hydraulic properties of geosynthetics after mechanical damage and abrasion laboratory tests. *Geosynthetics International*, **20**, No. 5, 358–374.

Rowe, R. K., Rimal, S. & Sangam, H. (2009). Ageing of HDPE geomembrane exposed to air, water and leachate at different temperatures. *Geotextiles and Geomembranes*, **27**, No. 2, 137–151.

Santos, E. C. G. (2007). *Application of Recycled Construction and Demolition Waste (RCDW) in Reinforced Soil Structures*. Masters Degree Dissertation, Geotechnical Engineering Department, School of Engineering of University of São Paulo at São Carlos, University of São Paulo, São Carlos, São Paulo, Brazil (in Portuguese).

Santos, E. C. G. & Vilar, O. M. (2008). Use of recycled construction and demolition wastes (RCDW) as backfill of reinforced soil structures. *Proceedings of the 4th European Conference on Geosynthetics*, Dixon N., Editor, International Geosynthetic Society, Edinburgh, UK, 1–8.

Santos, E. C. G., Vilar, O. M. & Assis, A. P. (2009). Statistical analysis of geotechnical parameters of recycled construction and demolition waste (RCDW). *Proceedings of the 17th International Conference on Soil Mechanics and Geotechnical Engineering*, Hamza, M., Shahien, M. & El-Mossallamy, Y., Editors, IOS Press, Alexandria, Egypt, vol. 5, pp. 1–4.

Santos, E. C. G., Palmeira, E. M. & Bathurst, R. (2010). Construction of a full-scale wrapped face geogrid reinforced wall using recycled construction and demolition waste as backfill material. *Proceedings of the 9th International Conference on Geosynthetics*, Palmeira, E. M., Vidal, D. M., Sayão, A. S. J. F. & Ehrlich, M., Editors, International geosynthetic Society – Brazil (IGS-Brazil), Guarujá, São Paulo, Brazil, pp. 1769–1772.

Santos, E. C. G., Bueno, B. S. & Palmeira, E. M. (2012). Strength reduction of geosynthetics used in RSW built with RCDW as backfill material. *Proceedings of the 5th European Conference on Geosynthetics*, Leiro, A., Editor, International Geosynthetic Society – Spain, Valencia, Spain, pp. 481–485.

Santos, E. C. G., Palmeira, E. M. & Bathurst, R. (2013). Behaviour of a geogrid reinforced wall built with recycled construction and demolition waste backfill on a collapsible foundation. *Geotextiles and Geomembranes*, **39**, No. 1, 9–19.

Santos, E. C. G., Palmeira, E. M. & Bathurst, R. (2014). Performance of two geosynthetic reinforced walls with recycled construction waste backfill and constructed on collapsible ground. *Geosynthetics International*, **21**, No. 4, 256–269.

Silva, R. V., Brito, J. & Dhir, R. K. (2014). Properties and composition of recycled aggregates from construction and demolition waste suitable for concrete production. *Construction and Building Materials*, **65**, 201–217.

Soleimanbeigi, A., Tanyu, B. F., Aydilek, A. H., Florio, P., Abbaspour, A., Dayioglu, A. Y. & Likos, W. J. (2019). Evaluation of recycled concrete aggregate as backfill for geosynthetic-reinforced MSE walls. *Geosynthetics International* **26**, No. 4, 396–412.

Taherkhani, H. (2015). Evaluation of the physical properties of unbound base layer containing recycled aggregates. *International Journal of Environmental Science and Development*, **6**, No. 4, 279–285.

Tognon, A. R., Rowe, R. K. & Moore, I. D. (2000). Geomembrane strain observed in large-scale testing of protection layers. *Journal of Geotechnical and Geoenvironmental Engineering*, **126**, No. 12, 1194–1208.

Vieira, C. S. & Pereira, P. M. (2015a). Damage induced by recycled construction and demolition wastes on the short-term tensile behaviour of two geosynthetics. *Transportation Geotechnics*, **4**, 64–75.

Vieira, C. S. & Pereira, P. M. (2015b). Use of recycled construction and demolition materials in geotechnical applications: a review. *Resources, Conservation and Recycling*, **103**, 192–204.

Vieira, C. S. & Pereira, P. M. (2016). Interface shear properties of geosynthetics and construction and demolition waste from large-scale direct shear tests. *Geosynthetics International*, **23**, No. 1, 62–70.

Vieira, C. S., Pereira, P. M. & Lopes, M. L. (2016). Recycled construction and demolition wastes as filling material for geosynthetic reinforced structures. *Interface properties. Journal of Cleaner Production*, **124**, 299–311.

Yoo, H., Jeon, H. Y. & Chang, Y. C. (2009). Evaluation of engineering properties of geogrids for soil retaining walls. *Textile Research Journal*, **80**, No. 2, 184–192.

The Editor welcomes discussion on all papers published in Geosynthetics International. Please email your contribution to discussion@geosynthetics-international.com by 15 June 2020.